Two-Effects-in-One: Kinetic Quantum and Molecular Sieving Effect in a Robust-Flexible [Th6Co2] Cage for both Isotope and Isomer Separation

Mengjia Yin
East China University of Technology
Rajamani Krishna
University of Amsterdam https://orcid.org/0000-0002-4784-8530
Wenjing Wang
Fujian Institute of Research on the Structure of Matter, Chinese Academy of Sciences
Daqiang Yuan
Fujian Institute of Research on the Structure of Matter https://orcid.org/0000-0003-4627-072X
Yaling Fan
East China University of Technology
Xuefeng Feng
East China University of Technology
Li Wang
East China University of Science and Technology
Feng Luo (ecitluofeng@163.com)
East China University of Technology https://orcid.org/0000-0001-6380-2754

Article

Keywords: Cage-based Compound, Hydrogen Isotope Separation, Robust-flexible Adsorption, Isomer Separation

Posted Date: November 9th, 2020

DOI: https://doi.org/10.21203/rs.3.rs-99357/v1

Abstract

Although molecular and quantum sieving (MS and QS) effects have been realized and employed to execute separation tasks, however, little is known about the coexistence of both effects in a compound and its corresponding structure. In this work, we show the first observation of coexistence of both quantum and molecular sieving effects in a [Th6Co2] cage-based compound (Th-Co-Cage-1). The [Th6Co2] cage shows 0.78 nm aperture but with an irregular crescent-like window. This allows [Th6Co2] cage to give ultrahigh uptake for hydrogen isotope and selectivity towards D2 over H2, leading to complete hydrogen isotope separation, as evidenced by experimental breakthrough test. When the size of guest molecule is more than the crescent-like window, a highly rare robust-flexible adsorption was observed, consequently leading to complete isomer separation for C4 and C6 isomers through molecular sieving effect. High thermal, water and chemical stability further supports the materials for practical separation application. The results open up a gate of material with coexistence of QS and MS effects and its fundamental design for superior separation application.

Introduction

Cages involved in organic cages and coordination-driven cages containing inherent inner porosity present a highly desired porous material for host-guest recognization and separation.[1-7] The pore of cages is also very special and composed of two major factors, *viz.* inner aperture that generally related to the accommodating capacity for guest molecules, and window size that determines the entrance size for guest molecules. Accordingly, cages could be a good candidate to perform molecular sieving effect for separation. When the window size becomes small enough to generate a confinement system, then the kinetic quantum sieving (KQS) effect was observed.[8,9]

Separation is an important chemical industrial process and now provides almost all purity matters for us from corresponding mixture.[10] The mature technique for separation is based on boiling-point-different distillation method, however, which not only requires huge capital investment, but also consume extensive energy, accounting for 10-15% of energy consumed worldwide.[10] By contrast, porous adsorbent based pathway is relatively low-cost and energy-saving and is now receiving increasing attention.[11-17] And several porous adsorbents involving in traditional zeolite and porous carbon, and newly developed metal-organic framework, cage compounds, hydrogen-bonded framework, and covalent organic frameworks have been attested to be effective for separating certain mixtures such as CO_2/N_2, C_2H_2/CO_2, C_2H_2/C_2H_4, C_2H_4/C_2H_6, SO_2/CO_2, and Xe/Kr.[18-24]

Among these separations, both isotope and isomer separation are highly desirable but extremely challenging, due to their urgent and plentiful demand and nearly identical physicochemical properties. For example, deuterium (D), an isotope isomer of H, is of prime importance in utilizing nuclear fusion reactors, whereas isomer separation such C_6 separation is of extreme importance in upgrading gasoline. Both of them play an important role in resolving energy crisis.

As suggested by theoretical and experimental results, production of D from D/H separation upon porous adsorbents can be overcome through both kinetic quantum sieving (KQS) and chemical affinity quantum sieving (CAQS) effect.[8,9,25-32] KQS just occurs within a very small confined space or entrance, which can then lead to different transport between D and H, due to their difference in de Broglie wavelength. Correspondingly, CAQS is generally dominated by open-metal site that affords distinct affinity towards D and H. Due to the extremely small size of D_2 and H_2 (dynamic diameter 2.89 Å), KQS often requires ultrafine pore with aperture or entrance around 3 Å (Scheme 1), however, this typically leads to materials with low pore volumes, and consequently low D_2 adsorption capacity, thus making such processes difficult in industrial application.

On the other hand, isomer separation in principle can be figured out upon the discrepancy in molecular size of isomers through molecular sieving (MS) effects of porous adsorbents.[33] As we know, the smallest molecule with isomer phenomenon is C_4 molecules, for example, n-butane *vs. iso*-butane, where n-butane and *iso*-butane give dynamic diameter of 4.7 Å and 5.3 Å, respectively. Thereby, generally isomer separation *via* MS effect requires microporous pore with aperture or entrance more than 4.5 Å (Scheme 1). Interestingly, when the pore meets the criterion of MS for isomer separation, however it will largely reduce and even eliminate KQS, and *vice versa*, and thereby, there brings an interestingly scientific concern of whether KQS and MS can coexist in one material.

To answer this concern, we synthesized a $[Th_6Co_2]$ cage compound, which shows a special crescent-like window with continuous varying size, but big inner aperture, meeting the dual standard for both KQS and MS, as well as industrial practice demand (big pore volume along with high adsorption capacity). Both single component adsorption tests and breakthrough experiments confirm its superior application in D/H, and C_4, C_6 isomer separation.

Results

Th-Co-Cage-1 ($[Th_2Co_2L_6]$, L^{2-}=5-(1H-imidazol-1-yl)isophthalate) was synthesized by the solvothermal reaction of $Th(NO_3)_4$, $Co(NO_3)_2$, and L in DMF with present of HNO_3 at 120°C. The yield is up to 90% based on Th. Single crystal X-ray diffraction reveals that **Th-Co-Cage-1** crystallizes in the rhombohedral crystal system with *R-3c* space group. In the asymmetry unit there is one crystallography-independent Th and Co site. The Th(IV) site is coordinated by nine carboxylate oxygen atoms from six L^{2-} ligands, while the Co(II) site holds the common octahedral geometry finished by three carboxylate oxygen atoms from three L^{2-} ligands and three nitrogen atoms from other three L^{2-} ligands. Each L^{2-} ligand connects to two Th(IV) ions and two Co(II) ions with one carboxylate in the chelate mode and the other one in the bridging mode. The secondary building unit in **Th-Co-Cage-1** is the unique $[Th_6Co_2]$ nanocage (Figure 1a, 1b, 1c), showing an elongated hexagonal bipyramid configuration, finished by six Th(IV) ions creating hexagon, and two Co(II) ions as vertex up and down. The effective aperture excluded the *van der* Waals Radii of

atoms is ca. 7.8 Å. Each cobalt vertex connects to the middle hexagon through three L^{2-} ligands. Due to the non-symmetrical L^{2-} ligands *plus* big distortion of imidazol fragment of L^{2-} ligands (dihedral angle of ca. 39° between imidazol and phenyl sections), an irregular crescent-like window showing continuous varying size was observed for this [Th_6Co_2] cage. The three-dimensional structure was generated through co-sharing two Th(IV) ions among two adjacent cages (Figure 1c). The topology matrix can be obtained by considering each CoTh dinuclear (connected by three carboxylate groups of L^{2-} ligands) and L^{2-} ligand to be nine-connected node (Figure S1) and three-connected node (Figure S2), respectively, resulting in an overall ftw-type topology (Figure 1d).[34] The solvent-accessible volume is estimated to be 41.5% of the cell volume.[35] Impressively, as discussed above, the unique structure feature in this [Th_6Co_2] cage showing big cavity but irregular crescent-like window with continuous varying size strongly suggests its potential with coexistence of both KQS and MS and thus superior applications in both isotope and isomer separation.

The thermal stability of **Th-Co-Cage-1** was initially investigated by thermogravimetric analysis (TG), giving the loss of solvent molecules before 340 °C (Figure S3). Notably, this MOF displays ultrahigh thermal and chemical stability (Figure 2), for example calcination at 350 °C for 24 h, immersion in water or boiling water for 7 d, as well as immersion in acidic or alkaline solution at pH=3-12 for 24 h. After methanol exchange the activated samples were obtained by 150°C under vacuum. A typical type I profile of N_2 adsorption at 77 K was observed for the activated samples (Figure S4). The BET surface area and pore volume is 717 m^2/g and 0.29 cm^3/g. A narrow pore size distribution at 0.76 nm is observed, well consistent with the aperture (0.78 nm) of [Th_6Co_2] cage estimated from structure.

To confirm our claim, we first explored isotope separation such as D_2/H_2 separation. As shown in Figure 3a, **Th-Co-Cage-1** enables ultrahigh D_2 adsorption capacity up to 208 cm^3/g at 1 bar and 77 K, respectively, exceeding benchmark porous adsorbents for D/H separation such as zeolite 5A (91.8 cm^3/g),[36] porous organic cage of cocryst1 (107 cm^3/g),[8,9] and MFU-4l (186 cm^3/g).[37] By contrast, H_2 uptake at similar condition is 186 cm^3/g, lower than D_2 uptake about 22 cm^3/g, indicative of selective adsorption of D_2 than H_2, mainly due to that the heavier isotope of D_2 has lower zero energy and smaller de Broglie wavelength as compared to H_2. Notably, this extremely high adsorption capacity will be very important for industrial large-scale D_2/H_2 separation. To evaluate the affinity between cage and hydrogen isotopes, we further carried out calculation of adsorption enthalpies (Q_{st}) for D_2 and H_2 by Viral equation, in light of adsorption isotherm data at 77 and 87 K (Figure S5), giving 8.4 kJ/mol for D_2, stronger than 7.9 kJ/mol for H_2 at zero coverage (Figure S6). The selective adsorption of D_2 over H_2 was then evaluated by the ideal adsorption solution theory (IAST),[38-40] giving D_2/H_2 selectivity of 1.38 for an equimolar D_2/H_2 mixture at 77 K and 1 bar (Figure S7), comparable with the famous MOF of HKUST-1 (S=1.42).[28] To further confirm the D_2/H_2 separation ability, dynamic breakthrough experiments upon **Th-Co-Cage-1** bed were performed at 77 K and 1 bar for a H_2/D_2/Ne (10/10/80, vol.%) mixture. Impressively, H_2 was first to

eluted through the packed column, whereas the retention time for D_2 is about 10 min/g, suggesting complete D_2/H_2 separation (Figure 3b). The separation ability is comparable with HKUST-1 (10 min/g) at the same conditions,[28] where the separation mechanism results from the CAQS effect from open Cu(II) site. As discussed above, within this [Th_6Co_2] cage, both Th and Co ions are fully coordinated by L^{2-} ligands, excluding possibility of providing an open metal site for host-guest recognization and thus CAQS effect. Accordingly, KQS effect could be responsible for the D_2/H_2 separation in **Th-Co-Cage-1**, and from the viewpoint of structural feature, this claim is reasonable, as this [Th_6Co_2] cage shows an irregular crescent-like window with continuous varying size indeed involved in a very narrow window around 2.9 Å that meets the criterion to occur of KQS effect.

After confirming the validity of isotope separation by **Th-Co-Cage-1**, we next explore the use of this material for isomer separation. Firstly, C_4 of n-butane and *iso*-butane was selected based on the consideration of their dynamic diameter of 4.7 Å and 5.3 Å, respectively, where the size of n-butane is comparable with the big window of [Th_6Co_2] cage, whereas the size of *iso*-butane is bigger than the big window of [Th_6Co_2] cage, thus making a possibility of MS effect for isomer separation. As expected, the single-component adsorption experiments show that the adsorption capacity of n-butane is as high as 3.5 mmol/g, whereas *iso*-butane is somewhat excluded from [Th_6Co_2] cage with just low uptake of 1.2 mmol/g at 1 bar and 298 K (Figure 3c). The n-butane uptake is far exceeding most reported porous adsorbents such as ZU-36-Co (2.1 mmol/g),[41] Y-fum-fcu-MOFs (2.0 mmol/g),[42] and commercial shaped 5A zeolite (1.3 mmol/g).[41] Seem form the adsorption isotherms, n-butane adsorbed steeply at low pressure below 0.02 bar, then an abrupt junction was observed, and following adsorption also becomes steep, fully agreeing with the recently defined robust-flexible adsorption.[43,44] However, this phenomenon is not observed for *iso*-butane adsorption. As we konw, n-butane gives dynamic diameter of 4.7 Å, slightly larger than the window of [Th_6Co_2] cage (big window of 4.4Å), and thus occurrence of robust-flexible adsortion is reasonable. While for branched isomer of *iso*-butane, it owns bigger dynamic diameter of 5.3 Å, far exceeding the window of [Th_6Co_2] cage, resulting in normal MS effect and consequently low uptake. To further confirm this robust-flexible adsortion, we next measured the adsorption of C_3H_6 that also owns a dynamic diameter of 4.7 Å. Similarly, Figure S8 shows the typical robust-flexible adsorption for C_3H_6. First a steep adsorption at 0-2.5 kPa was observed, then a step adsorption indicating a gate-opening behavior was followed. The overall C_3H_6 adsorption agrees well with the reported definition of robust-flexible MOF such as UTSA-300 and ELM-12.[37] To our best of knowledge, only extremely few robust-flexible compounds were reported until now. Our case should present the first actinides-based compounds with robust-flexible adsorption. For both n-butane and C_3H_6, they hold slight larger kinetic diameter than the window of [Th_6Co_2] cage, thus rationally resulted in the gate-opening behavior. In this regard, we can draw a conclusion that robust-flexible adsorption will be absent for molecule smaller than the window of the [Th_6Co_2] cage. As expected, **Th-Co-Cage-1** preforms high C_2H_4 uptake of 3.67 mmol/g at 1 bar and 298 K, however the adsorption isotherm of C_2H_4 is distinct from that for n-butane and C_3H_6,

excluding the robust-flexible nature (Figure S8), owing to C_2H_4 molecule with a smaller kinetic diameter of 4.2 Å.

The separation ability of C_4 isomer was initially reflected on the high n-butane/*iso*-butane selectivity, giving n-butane/*iso*-butane selectivity up to 130.5 at 1 bar and 298 K for an equimolar n-butane/*iso*-butane mixture (Figure S9). The results imply its outstanding potential in n-butane/*iso*-butane separation. Whereafter, to assert the actual separation potential, breakthrough experiments upon **Th-Co-Cage-1** bed was carried out for an equimolar n-butane/*iso*-butane mixture at 298 K (Figure 3d). As expected, *iso*-butane breaks out the column immediately, suggesting that the *iso*-butane adsorption was completely excluded by **Th-Co-Cage-1**, owing to MS effect, well consistent with the adsorption results and structural analysis. By contrast, n-butane can be retained in **Th-Co-Cage-1** column for a very long time up to 70 min/g. The n-butane adsorption capacity is as high as 3.25 mmol/g, equal to 97% of the theoretic adsorption capacity (3.35 mmol/g at 0.5 bar). This value is far exceeding the benchmark material of ZU-36-Co (0.89 mmol/g).[41] The production of pure *iso*-butane (>99.9%) is as high as 68 mL/g, also far exceeding the benchmark material of ZU-36-Co (17.5 mL/g).[41] The results strongly suggest its superior application in C_4 isomer separation.

Furthermore, separation of C_6 isomer was carried out. For C_6 isomer separation, complete separation of linear, monobranched and dibranched isomers are still a challenging task.[33] Regarding the kinetic diameter of C_6 isomers shows the order of n-HEX (n-hexane, 4.3Å)<3MP(3-methylpentane, 5.0 Å)=2MP(2-methylpentane, 5.0 Å)<23DMB (2,3-dimethylbutane, 5.6 Å) <22DMB(2,2-dimethylbutane, 6.2 Å), in conjunction with the robust-flexible adsorption in this [Th_6Co_2] cage, complete separation of linear, monobranched and dibranched isomers by **Th-Co-Cage-1** can be expected. Accordingly, we then measured C_6 vapour adsorption at 30 °C and the results were shown in Figure 3e. Ultrahigh n-HEX adsorption capacity up to 209 mg/g was observed, exceeding most top level materials for this task[45-53] such as Al-bttotb (151 mg/g),[49] Ca-tcpb (150 mg/g),[48] MIL-53(Fe)-$(CF_3)_2$ (32 mg/g),[47] and $Fe_2(BDP)_3$ (113 mg/g)[46]. By contrast, no adsorption and very low adsorption of 10.7 mg/g was observed for the dibranched isomers of 22DMB and 23DMB, owing to MS effect, since the kinetic diameter of dibranched isomers is far larger than the window of [Th_6Co_2] cage. Impressively, moderate uptake of 93.2 mg/g and 93.8 mg/g for monobranched 3MP and 2 MP was observed, most likely due to the unique robust-flexible nature in this material, as both 3 MP and 2 MP owns comparable kinetic diameter with C_3H_6 and n-butane molecules that shows typical robust-flexible adsorption as discussed above. The results suggest potential complete separation among linear, monobranched, and dibranched isomers. We further carried out the adsorption kinetics. As shown in Figure S10, **Th-Co-Cage-1** shows high n-HEX uptake, moderate 2 MP and 3 MP uptake, low 23DMB uptake, and no uptake for 22DMB, which is well consistent with the adsorption isotherm. The adsorption equilibrium time is within 100 s for these isomers. Impressively, the adsorption kinetics also shows some difference for monobranched isomers of 2MP and 23DMB, or dibranched isomers of 23DMB and 22DMB, implying an outstanding potential for total separation of C_6 isomers.

To confirm the practical separation capability, we next carried out a series of batch experiments from a binary, or ternary, or quaternary mixture in liquid phase (Table 1, Figure S11-20). In the literature, all reports are focused on the separation of C_6 vapour *via* multicomponent column breakthrough measurements.[45-53] From the viewpoint of saving energy, the direct separation of C_6 isomer from liquid mixture is more desirable, as these C_6 isomers are essentially liquid at room temperature with boiling point more than 58°. In each case, the activated **Th-Co-Cage-1** samples were first immersed in commercially binary mixture. Then their contents were extracted by n-butyl acetate from the samples after drying naturally. Impressively, 100% pure liner n-HEX or monobranched 2MP/3MP can be obtained from the binary linear/monobranched, or linear/dibranched, or monobranched/ dibranched mixture. More importantly, 100% pure 3MP can also be obtained from the 2MP/3MP mixture. Similar trend is also observed for the ternary mixture, yielding the 100% pure n-HEX or 3MP from the n-HEX/3MP/2,2DMB or 3MP/2MP 2,2DMB mixture, respectively. Besides, 100% n-HEX can be generated from the quaternary n-HEX/3MP/2MP/2,2DMB mixture. All the above results strongly suggest complete separation of C_6 isomer with 100% pure linear or monobranched product. Moreover, the production ability is also attractive. For example, 160 mg/g, 140 mg/g, and 110 mg/g pure n-HEX can be yielded from the n-HEX/3MP, or n-HEX/3MP/2,2DMB, or n-HEX/3MP/2MP/ 2,2DMB mixture, while 46 mg/g pure 3MP was produced from a 3MP/2,2DMB mixture. Even for 3MP/2MP mixture, a high production for 3MP up to 58 mg/g was observed. To further confirm the practical separation capability, we also for the first time carried out the direct separation *via* multicomponent column breakthrough measurements with the liquid phase mixture (Figure 3f). The results show that **Th-Co-Cage-1** can well separate the C_6 mixture into individual components. 22DMB breaks firstly from Th-Co-MOF bed after 24 s/g, then the retention time for 2MP, 3MP and n-HEX is 42 s/g, 58 s/g, and 72 s/g, respectively.

Table 1. A summary of C_6 separation upon **Th-Co-Cage-1**.

Entry	n-HEX	2MP	3MP	22DMB	Product	Purity (%)	Capacity (mg/g)
1	√	√			n-HEX	>99.9%	150
2	√		√		n-HEX	>99.9%	160
3	√			√	n-HEX	>99.9%	130
4		√	√		3MP	>99.9%	58
5		√		√	2MP	>99.9%	38
6			√	√	3MP	>99.9%	46
7	√		√	√	n-HEX	>99.9%	140
8		√	√	√	3MP	>99.9%	60
9	√	√	√	√	n-HEX	>99.9%	110

Discussion

In summary, we have successfully obtained the first case showing coexistence of KQS and MS effects. Different from the generally encountered porous materials with regular pore, the underlying material is a cage compound showing irregular crescent-like window with continuous varying size, which fully meets the dual criterion for both KQS and MS effects. Consequently, this cage compound can effectively separate not only size-equal molecules such as D/H isotope, but also size-distinct molecules such as C_4 and C_6 isomers.

References

1. Rowland, C. A. et al. Methane storage in paddlewheel-based porous coordination cages. *J. Am. Chem. Soc.* **140**, 11153–11157 (2018).
2. Liu, Y. et al. Chloride capture using a C-H hydrogen-bonding cage. *Science.* **365**, 159–161 (2019).
3. Tromans, R. A. et al. A biomimetic receptor for glucose. *Nat. Chem.***11**, 52–56 (2019).
4. Liu, M. et al. Barely porous organic cages for hydrogen isotope separation. *Science.* **366**, 613–620 (2019).
5. Sun, N. et al. Multifunctional Tubular Organic Cage-Supported Ultrafine Palladium Nanoparticles for Sequential Catalysis. *Angew. Chemie Int. Ed.* **58**, 18011–18016 (2019).
6. Giri, N. et al. Liquids with permanent porosity. *Nature.* **527**, 216–220 (2015).
7. Gosselin, E. J. et al. Permanently Microporous Metal-Organic Polyhedra. *Chem. Rev.* **120**, 8987–9014 (2020).

8. Liu, M. et al. Barely porous organic cages for hydrogen isotope separation. *Science.* **366**, 613–620 (2019).
9. Schneider, M. W. et al. Post-Modification of the Interior of Porous Shape-Persistent Organic Cage Compounds. *Angew. Chem. Int. Ed.* **52**, 3611–3615 (2013).
10. Sholl, D. S. et al. Seven chemical separations to change the world. *Nature.* **532**, 435-437 (2016).
11. Lin, R. B. et al. Exploration of porous metal–organic frameworks for gas separation and purification. *Coord. Chem. Rev.* **378**, 87-103 (2019).
12. Cui, X. et al. Pore chemistry and size control in hybrid porous materials for acetylene capture from ethylene. *Science.* **353**, 141-144 (2016).
13. Yang, S.; et al. Supramolecular binding and separation of hydrocarbons within a functionalized porous metal-organic framework. *Nat. Chem.* **7**, 121-129 (2015).
14. Liao, P. Q. et al. Efficient purification of ethene by an ethane trapping metal-organic framework. *Nat. Commun..* **6**, 1-9 (2015).
15. Lin, R. B. et al. Molecular sieving of ethylene from ethane using a rigid metal-organic framework. *Nat. Mater.* **17**, 1128 -1133 (2018).
16. Cadiau, A. et al. A metal-organic framework-based splitter for Separating propylene from propane. *Science.* **353**, 137-140 (2016).
17. Banerjee, D. et al. Xenon gas separation and storage using metalorganic frameworks. *Chem.* **4**, 466-494 (2018).
18. Wang, H. et al. Topologically guided tuning of Zr-MOF pore structures for highly selective separation of C_6 alkane isomers. *Nat. Commun.* **9**,1-11 (2018).
19. Cui, W. G. et al. Metal-organic framework materials for the separation and purification of light hydrocarbons. *Adv. Mater.* **31**, 1806445 (2019).
20. Chen, K. J. et al. Synergistic sorbent separation for one-step ethylene purification from a four-component mixture. *Science.* **366**, 241-246 (2019).
21. Zeng, H. et al. Induced fit of C_2H_2 in a flexible MOF through cooperative action of open metal sites. *Angew. Chem. Int. Ed.* **58**, 8515-8519 (2019).
22. Lin, R. B. et al. Multifunctional porous hydrogen-bonded organic framework materials. *Chem. Soc. Rev.* **48**, 1362-1389 (2019).
23. Li, Q. et al. Highly Selective Separation of Minimum-Boiling Azeotrope Toluene/Pyridine by Nonporous Adaptive Crystals of Cucurbit[6] uril. *Angew. Chem. Int. Ed.* **132**, 5393-5396 (2020).
24. Zou, L. et al. Porous organic polymers for post-combustion carbon capture. *Adv. Mater.* **29**,1700229 (2017).
25. Kim, J. Y. et al. Isotope Separation: Hydrogen Isotope Separation in Confined Nanospaces: Carbons, Zeolites, Metal-Organic Frameworks, and Covalent Organic Frameworks. *Adv. Mater.* **31**, 1970147 (2019).

26. Beenakker, J. J. M. et al. Molecular transport in subnanometer pores: zero-point energy, reduced dimensionality and quantum sieving. *Chem. Phys. Lett.* **232**, 379-382 (1995).
27. FitzGerald, S. A. et al. Highly selective quantum sieving of D_2 from H_2 by a metal-organic framework as determined by gas manometry and infrared spectroscopy. *J. Am. Chem. Soc.* **135**, 9458-9464 (2013).
28. Si, Y.; et al. Highly effective H_2/D_2 separation in a stable Cu-based metal-organic framework. *Nano. Res.* 1-8 (2019).
29. Noguchi, D. et al. Quantum sieving effect of three-dimensional Cu-based organic framework for H_2 and D_2. *J. Am. Chem. Soc.* **130**, 6367–6372 (2008).
30. Kim, J. Y. et al. Specific Isotope-Responsive Breathing Transition in Flexible Metal-Organic Frameworks. *J. Am. Chem. Soc.* **142**, 13278-13282 (2020).
31. Kim, J. Y. et al. Exploiting diffusion barrier and chemical affinity of metal-organic frameworks for efficient hydrogen isotope separation. *J. Am. Chem. Soc.* **139**, 15135-15141 (2017).
32. Zhang, L. et al. Exploiting Dynamic Opening of Apertures in a Partially Fluorinated MOF for Enhancing H_2 Desorption Temperature and Isotope Separation. *J. Am. Chem. Soc.* **141**, 19850-19858 (2019).
33. Wang, H. et al. Microporous metal–organic frameworks for adsorptive separation of C_5–C_6 alkane isomers. *Acc. Chem. Res.* **52**, 1968-1978 (2019).
34. Blatov, V. A. et al. TOPOS 4.0. Samara State University, Samara Oblast, Russia (1999) .
35. Spek, A. L. PLATON SQUEEZE: a tool for the calculation of the disordered solvent contribution to the calculated structure factors. *Acta. Cryst.* **71**, 9-18 (2015).
36. Xiong, R. et al. Thermodynamics, kinetics and selectivity of H_2 and D_2 on zeolite 5A below 77K. *Microporous Mesoporous Mater.* **264**, 22–27 (2018).
37. Teufel, J. et al. MFU-4-A Metal-Organic Framework for Highly Effective H_2/D_2 Separation. *Adv. Mater.* **25**, 635–639 (2013).
38. Xu, Z. et al. A robust Th-azole framework for highly efficient purification of C_2H_4 from a $C_2H_4/C_2H_2/C_2H_6$ mixture. *Nat. Commun.* **11**, 3163 (2020).
39. Luo, F. et al. UTSA-74: a MOF-74 isomer with two accessible binding sites per metal center for highly selective gas separation. *J. Am. Chem. Soc.* **138**, 5678-5684 (2016).
40. Fan, C. B. et al. Significant Enhancement of C_2H_2/C_2H_4 Separation by a Photochromic Diarylethene Unit: A Temperature-and Light-Responsive Separation Switch. *Angew. Chem. Int. Ed.* **56**, 7900-7906 (2017).
41. Zhang, Z. et al. Highly efficient separation of linear and branched C_4 isomers with a tailor-made metal-organic framework. *AIChE Journal.* e16236 (2020).
42. Assen, A. H. et al. Ultra-Tuning of the Rare-Earth fcu-MOF Aperture Size for Selective Molecular Exclusion of Branched Paraffins. *Angew Chem Int Ed.* **54**, 14353-14358 (2015).

43. Li, L. et al. Flexible-robust metal-organic framework for efficient removal of propyne from propylene. *J. Am. Chem. Soc.* **139**, 7733-7736 (2017).
44. Wang, J. et al. Optimizing Pore Space for Flexible-Robust Metal-Organic Framework to Boost Trace Acetylene Removal. *J. Am. Chem. Soc.* **142**, 9744-9751 (2020).
45. Assen, A. H. et al. Ultra-Tuning of the Rare-Earth fcu-MOF Aperture Size for Selective Molecular Exclusion of Branched Paraffin. *Angew. Chem. Int. Ed.* **54**, 14353-14358 (2015).
46. Herm, Z. R et al. Separation of hexane isomers in a metal-organic framework with triangular channels. *Science.* **340**, 960-964 (2013).
47. Wang, H. et al. Topologically guided tuning of Zr-MOF pore structures for highly selective separation of C_6 alkane isomers. *Nat. Commun.* **9**, 1-11 (2018).
48. Wang, H. et al. One-of-a-kind: a microporous metal–organic framework capable of adsorptive separation of linear, mono-and di-branched alkane isomers via temperature-and adsorbate-dependent molecular sieving. *Energy Environ. Sci.* **11**, 1226-1231 (2018).
49. Yu, L. et al. Splitting Mono-and Dibranched Alkane Isomers by a Robust Aluminum-Based Metal-Organic Framework Material with Optimal Pore Dimensions. *J. Am. Chem. Soc.* **142**, 6925-6929 (2020).
50. Babarao, R. et al. Molecular Insight into Adsorption and Diffusion of Alkane Isomer Mixtures in Metal-Organic Frameworks. *J. Phys. Chem. B.* **113**, 9129-9136 (2009).
51. Bozbiyik, B. et al. Shape selective properties of the Al-fumarate metal–organic framework in the adsorption and separation of n-alkanes, iso-alkanes, cyclo-alkanes and aromatic hydrocarbons. *Phys. Chem. Chem. Phys.* **18**, 3294-3301 (2016).
52. Dubbeldam, D. et al. Computer-assisted screening of ordered crystalline nanoporous adsorbents for separation of alkane isomers. *Angew. Chem. Int. Ed.* **51**, 11867-11871 (2012).
53. Mendes, P. A. P. et al. A complete separation of hexane isomers by a functionalized flexible metal organic framework. *Adv. Funct. Mater.* **48**, 7666-7673 (2014).

Declarations

Acknowledgments

This work was supported financially by the National Natural Science Foundations of China (21966002, 21871047, 21861017), the Natural Science Foundation of Jiangxi Province of China (20181ACB20003), and the Training Program for Academic and Technical Leaders of Major Disciplines in Jiangxi Province (20194BCJ22010).

Author contributions

F. L. conceived the experiments, writing, and editing; M. J. Y., Y. L. F., L. W., and X. F. F. carried out experiments; W. J. W. and D. Q. Y. carried out the H/D breakthrough test; R.K. calculated the selectivity and

simulated the breakthrough.

Scheme

Scheme 1 is available in the Supplementary Files.

Figures

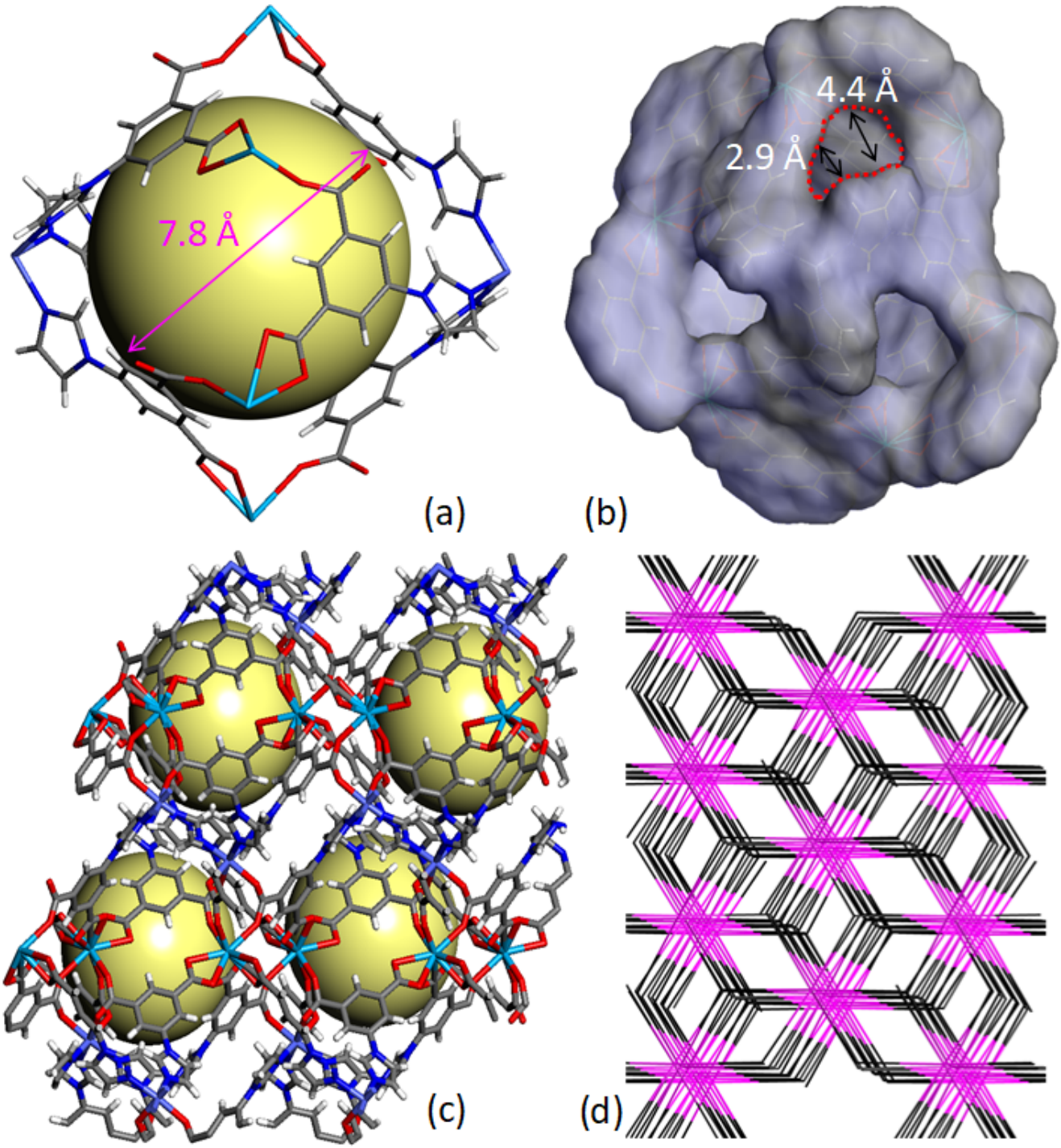

Figure 1

a) View of [Th6Co2] hexagonal bipyramid cage with the highlighted large cavity about 0.78 nm aperture. b) View of the Connolly surface of [Th6Co2] cage with an irregular crescent-like window showing continuous varying size (the highlighted size is stressed for D/H and isomer separation). c) View of the three-dimensional structure of [Th6Co2] cage compound. d) View of (3,9)-connected ftw topology for this [Th6Co2] cage compound.

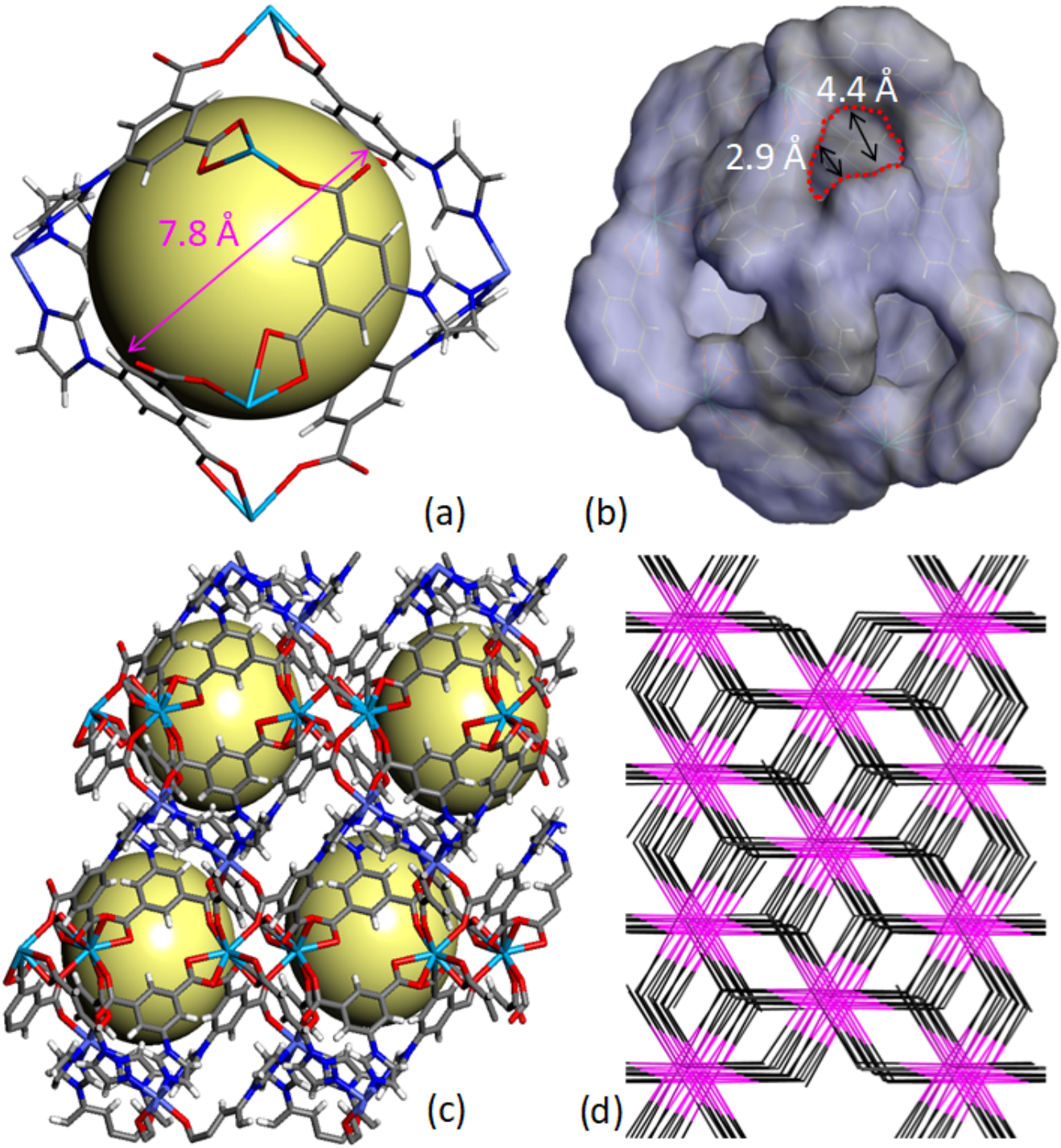

Figure 1

a) View of [Th6Co2] hexagonal bipyramid cage with the highlighted large cavity about 0.78 nm aperture. b) View of the Connolly surface of [Th6Co2] cage with an irregular crescent-like window showing continuous varying size (the highlighted size is stressed for D/H and isomer separation). c) View of the three-dimensional structure of [Th6Co2] cage compound. d) View of (3,9)-connected ftw topology for this [Th6Co2] cage compound.

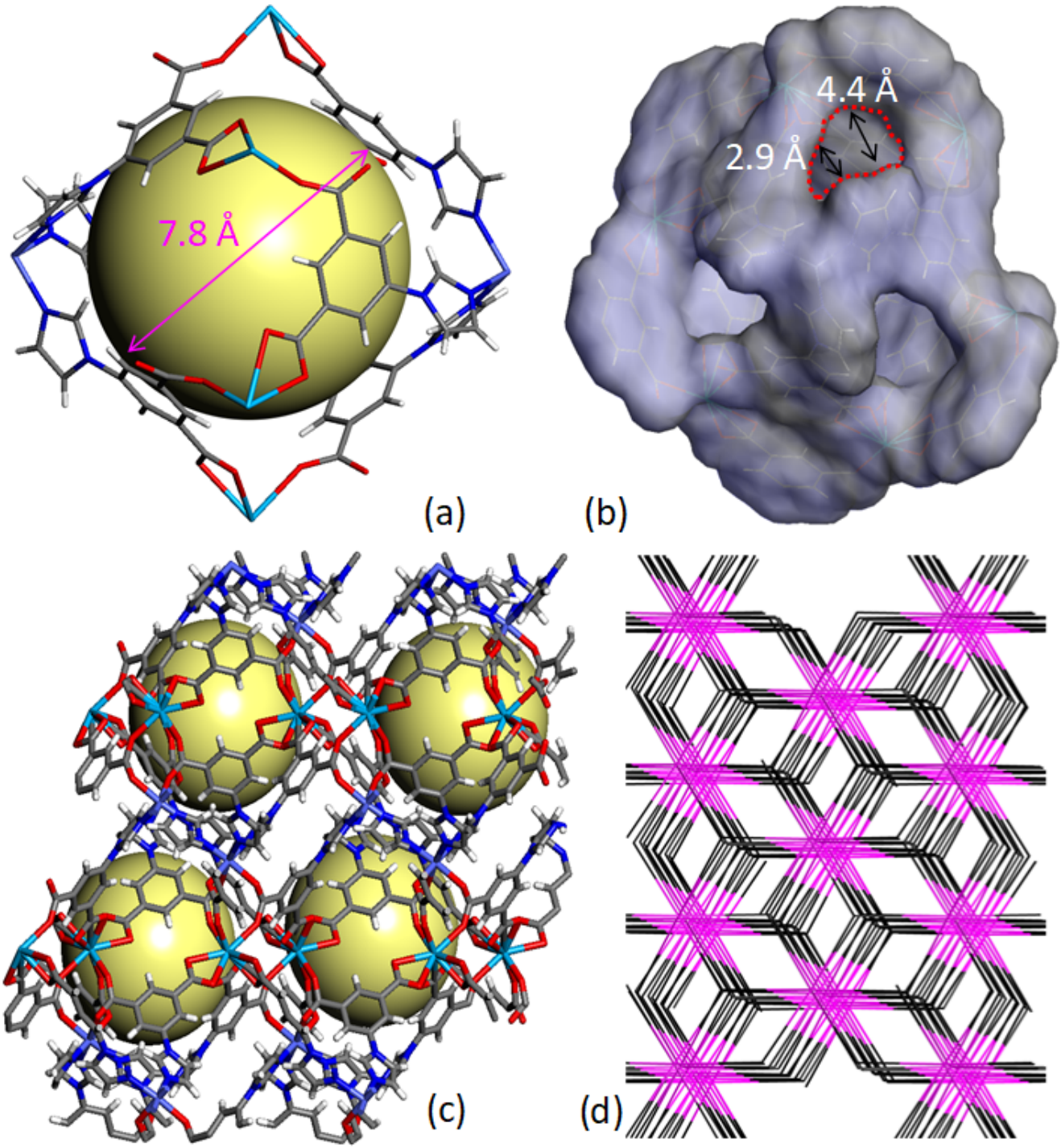

Figure 1

a) View of [Th6Co2] hexagonal bipyramid cage with the highlighted large cavity about 0.78 nm aperture. b) View of the Connolly surface of [Th6Co2] cage with an irregular crescent-like window showing continuous varying size (the highlighted size is stressed for D/H and isomer separation). c) View of the three-dimensional structure of [Th6Co2] cage compound. d) View of (3,9)-connected ftw topology for this [Th6Co2] cage compound.

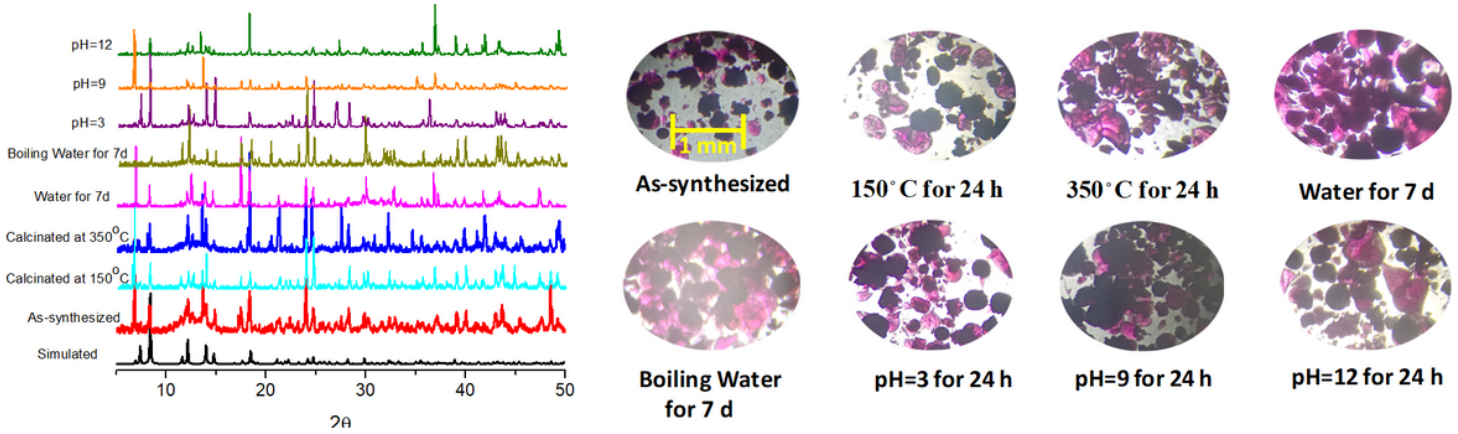

Figure 2

View of the PXRD patterns of the samples under different conditions and the simulated one from the single crystal data, as well as the photograph of the crystal under different conditions.

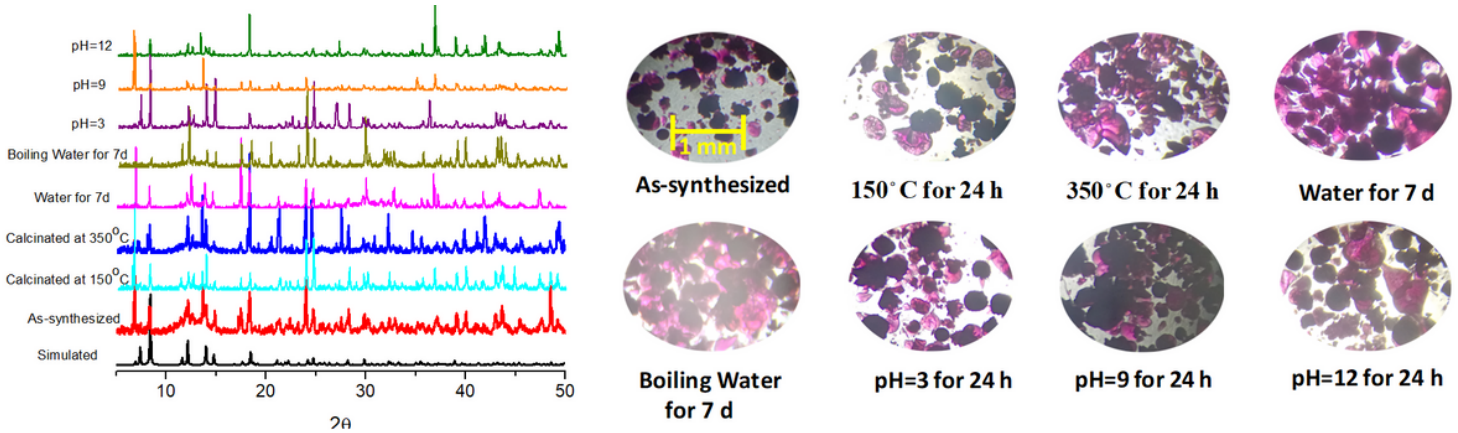

Figure 2

View of the PXRD patterns of the samples under different conditions and the simulated one from the single crystal data, as well as the photograph of the crystal under different conditions.

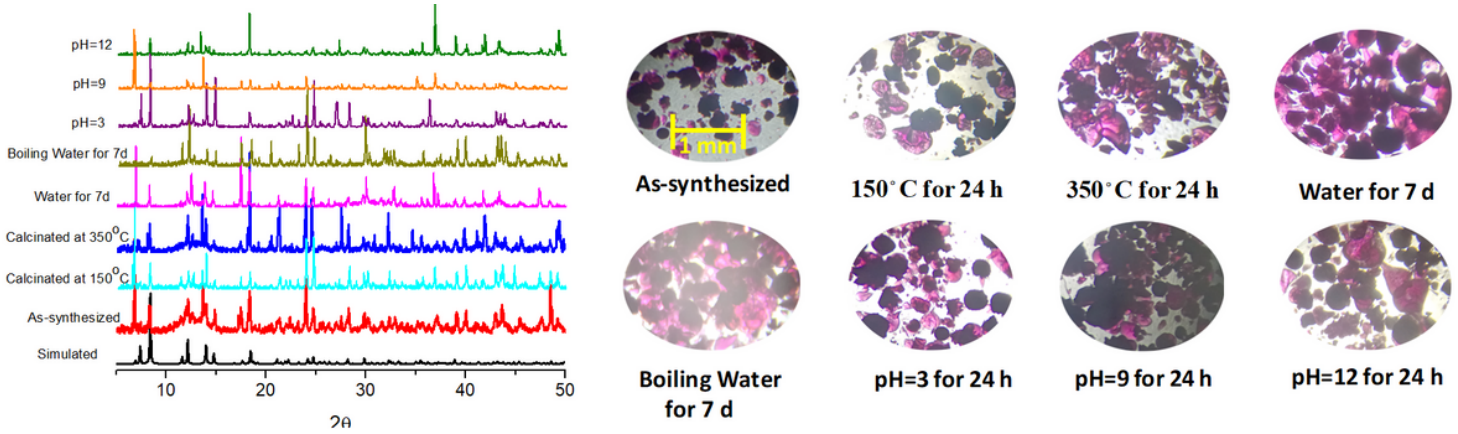

Figure 2

View of the PXRD patterns of the samples under different conditions and the simulated one from the single crystal data, as well as the photograph of the crystal under different conditions.

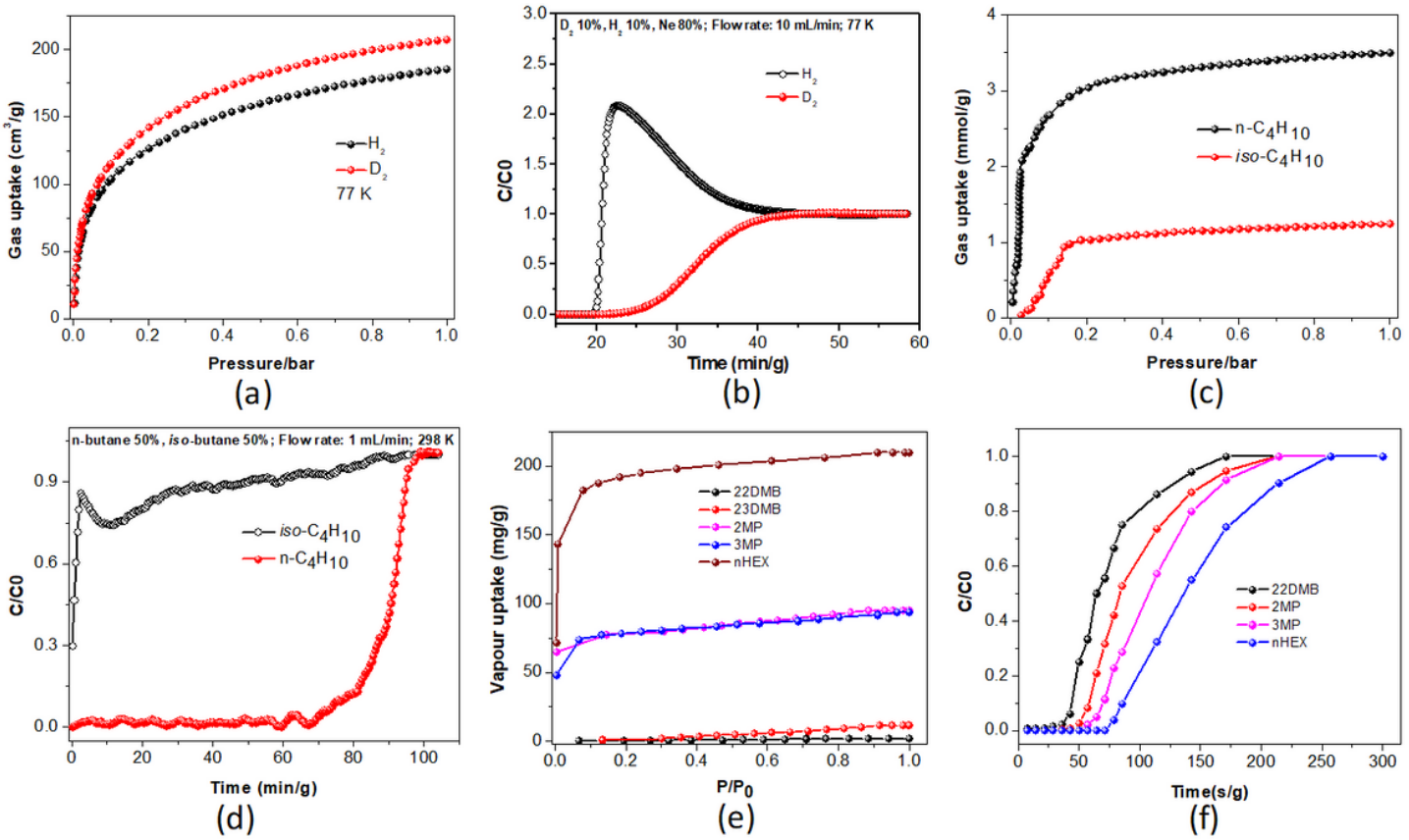

Figure 3

The adsorption and separation for both isotope and isomer explored in this work. (a) The D2 and H2 adsorption isotherms at 77 K. (b) The breakthrough experiments upon Th-Co-Cage-1 bed for D2/H2 separation. (c) The C4 isomer adsorption isotherms at 298 K. (d) The breakthrough experiments upon Th-Co-Cage-1 bed for C4 isomer separation at 298 K. (e) The C6 isomer adsorption isotherms at 303 K. (d) The breakthrough experiments upon Th-Co-Cage-1 bed for C6 isomer separation at 303 K.

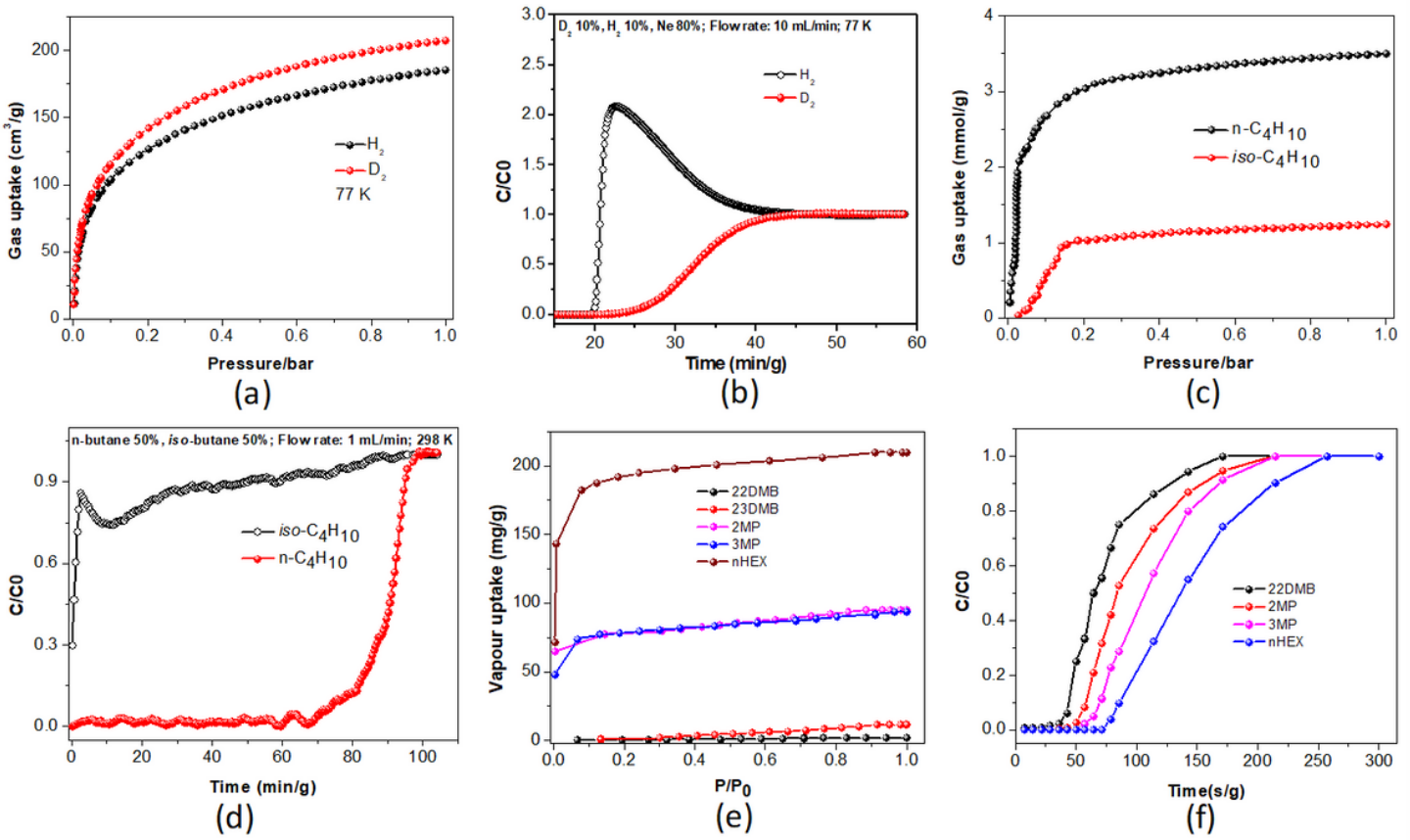

Figure 3

The adsorption and separation for both isotope and isomer explored in this work. (a) The D2 and H2 adsorption isotherms at 77 K. (b) The breakthrough experiments upon Th-Co-Cage-1 bed for D2/H2 separation. (c) The C4 isomer adsorption isotherms at 298 K. (d) The breakthrough experiments upon Th-Co-Cage-1 bed for C4 isomer separation at 298 K. (e) The C6 isomer adsorption isotherms at 303 K. (d) The breakthrough experiments upon Th-Co-Cage-1 bed for C6 isomer separation at 303 K.

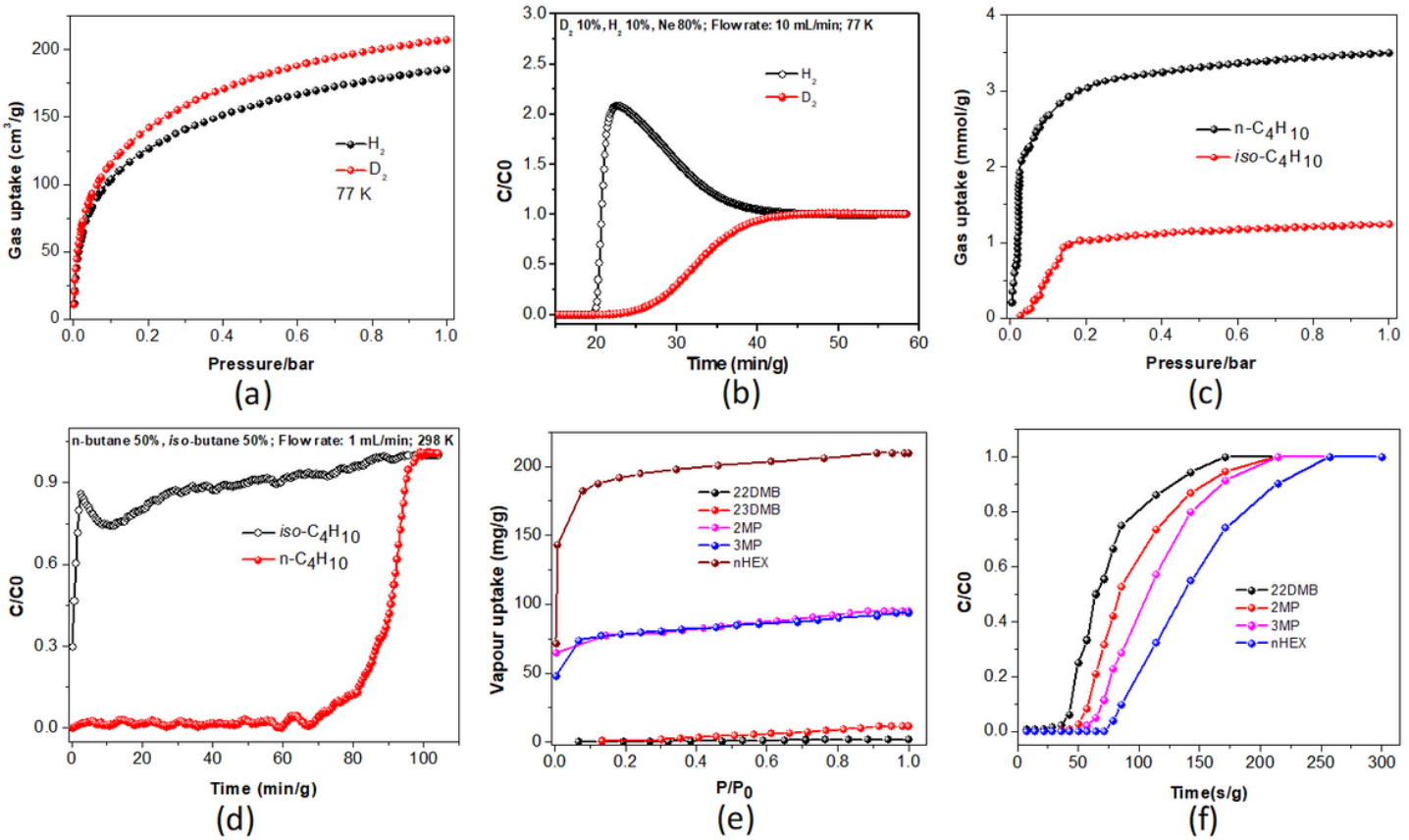

Figure 3

The adsorption and separation for both isotope and isomer explored in this work. (a) The D2 and H2 adsorption isotherms at 77 K. (b) The breakthrough experiments upon Th-Co-Cage-1 bed for D2/H2 separation. (c) The C4 isomer adsorption isotherms at 298 K. (d) The breakthrough experiments upon Th-Co-Cage-1 bed for C4 isomer separation at 298 K. (e) The C6 isomer adsorption isotherms at 303 K. (d) The breakthrough experiments upon Th-Co-Cage-1 bed for C6 isomer separation at 303 K.

Supplementary Files

This is a list of supplementary files associated with this preprint. Click to download.

- TOCGraphic.png
- TOCGraphic.png
- TOCGraphic.png
- Scheme1.png
- Scheme1.png
- Scheme1.png
- SI.docx
- SI.docx

- SI.docx